IEEE Transactions on Automatic Control, Volume 68, Issue 12, December 2023, pp. 7824-7831
DOI: 10.1109/TAC.2023.3247461

Closed-Loop Output Error Approaches for Drone's Physics Informed Trajectory Inference

Adolfo Perrusquía, *Member, IEEE*, Weisi Guo, *Senior Member, IEEE*

***Abstract*— The design of adequate countermeasures against drone's threats needs accurate trajectory estimation to avoid economic damage to the aerospace industry and national infrastructure. As trajectory estimation algorithms need highly accurate physics informed models or off-line learning algorithms, radical innovation in on-line trajectory inference is required. In this paper, a novel drone's physics informed trajectory inference algorithm is proposed. The algorithm constructs a physic informed model and infers the drone's trajectories simultaneously using a closed-loop output error architecture. Two different approaches are proposed based on a physics structure and an admittance filtering model which considers: i) full states measurements and ii) partial states measurements. Stability and convergence of the proposed schemes are assessed using Lyapunov stability theory. Simulations studies are carried out to demonstrate the scope and high inference capabilities of the proposed approach.**

***Index Terms*— physics informed model, trajectory inference, admittance model, drones, full/partial states measurements**

I. Introduction

PROLIFERATION of cheaper drone technology has magnified the threat space for autonomous vehicle attacks on critical national and international infrastructures, defence, and security facilities. Therefore, reliable detection of drones and identifying its intention is paramount. The challenge with current detection systems relies on stable and highly accurate trajectory inference algorithms for early threat detection [1].

Drone-detection mechanisms [2] are based on either audio, video, motion, thermal, radar, and radio-frequency detection methods which are able to detect drones in different scenarios and applications [3]–[6]. However, these methods depend on snapshots of data which do not capture the information of the continuous flight physics associated to the mission profile and intent, that is, they are based on data collected from different experiments which are not associated to the current trajectory. Therefore, state estimation [7] and inference algorithms [8] have been developed to provide a complete landscape of the drone's performance.

Most of the state estimation algorithms, e.g., Kalman filter and their variants [9], [10], are based on a trustworthy physics informed model (PIM) [11], [12], also known as model-based, that allows to estimate unknown states with noise attenuation capabilities [13], [14]. A wrong model may cause large estimation error and instability in the estimation process [15]. Other techniques are based on Gaussian processes that capture all the prior information [16], [17] that we have from the real system in the form of non-parametric function approximators, which allow to infer the drone's trajectories in future time steps [18]. Nevertheless, these methods are usually off-line or use reinforcement learning (RL) architectures for exploration purposes [19], [20] to achieve enough excitation. However, the control policy is fixed in threat detection algorithms and hence on-line Gaussian processes cannot be applied.

Other approaches that deal with trajectory inference problems are known as physics informed neural networks (PINNs) [21] and recurrent neural networks (RNNs) [22]. On the one hand, a PINN uses the PIM as regularization term to improve learning convergence and to penalize large weights. On the other hand, RNNs use series-parallel/parallel structures to model the system as the sum of a stable linear system with a multi-layer perceptron network. Whilst PINNs require a normalized PIM to obtain good results, the RNNs cannot guarantee weights convergence and thus, the neural approximation cannot serve as a PIM. One main issue of PIMs is founded on the parameter's knowledge assumption to obtain highly accurate inference results; otherwise, low accuracy or instability could be obtained in the final inference results due to the universal instability issue of neural networks [23].

Since trajectory inference algorithms need a high fidelity PIM to ensure good estimation results, then a parameter identification algorithm is required. However, parameter identification algorithms [24], [25] depends on states measurements that can be affected in presence of noise [26], [27]. Closed-loop input/output (CLIE/CLOE) architectures [28]–[30] have been developed for parameter identification that deals with the noise issue using well-tuned filters to estimate velocity and acceleration terms and construct a PIM; nevertheless, the filters can cause biased estimates and delays in the inferred trajectory. In addition, the CLIE algorithm is limited to a class of linear systems with linear control inputs [31], [32].

In view of the above, this paper reports a drone's physics informed algorithm for trajectory inference using a closed-loop output error technique. Two different inference algorithms are developed based on the available measurable states. The first approach constructs a PIM based on the drone's dynamic model and full states measurements assumption. The second approach constructs a PIM based on the solution of the

This work was supported by the Royal Academy of Engineering and the Office of the Chief Science Adviser for National Security under the UK Intelligence Community Postdoctoral Research Fellowship programme.

A. Perrusquía and Weisi Guo are with the School of Aerospace, Transport and Manufacturing, Cranfield University, Bedford, UK (e-mail: {Adolfo.Perrusquia-Guzman,Weisi.Guo}@cranfield.ac.uk).

drone's dynamic model using an admittance model filtering and partial states measurements. The main contributions of the work are the following: i) two novel physics informed models for trajectory inference based on a physics and admittance parameterizations, ii) noise attenuation and parameter estimates convergence are simultaneously guaranteed under the fulfilment of a persistent of excitation condition, iii) the approach does not require additional filtering methods or prior parameters knowledge, and iv) rigorous stability and convergence analysis are provided to justify the proposed approach.

The paper outline is as follows: Section II defines the PIM based on a physics parameterization. Section III reports the PIM based on an admittance parameterization. Section IV expands the scope of Section III with an admittance parameterization using nested filters. Section V reports the simulation studies using a quadcopter. The conclusions are presented in Section VI.

Throughout this paper, $\mathbb{N}$, $\mathbb{R}$, $\mathbb{R}^+$, $\mathbb{R}^n$, $\mathbb{R}^{n\times m}$ denote the spaces of natural numbers, real numbers, positive real numbers, real n-vectors, and real $n\times m$-matrices, respectively; $I_n \in \mathbb{R}^{n\times n}$ denotes an identity matrix; $\lambda_{\min}(A)$ and $\lambda_{\max}(A)$ denotes the minimum and maximum eigenvalues of matrix A, respectively; the norms $\|A\| = \sqrt{\lambda_{\max}(A^\top A)}$ and $\|x\|$ stand for the induced matrix and vector Euclidean norms, respectively; where $x \in \mathbb{R}^n$, $A, B \in \mathbb{R}^{n\times n}$ and $n, m \in \mathbb{N}$.

II. Closed-Loop Output Error Approach: A Physics Parameterization

Consider the following drone's dynamic model

$$\ddot{q} = M^{-1}[u - C(q,\dot{q})\dot{q} - F(\dot{q}) - G(q)] = \Phi^\top(q,\dot{q},u)\Theta \quad (1)$$

where $M \in \mathbb{R}^{n\times n}$ is a constant inertia matrix, $C(q,\dot{q}) \in \mathbb{R}^{n\times n}$ denotes the Coriolis and centripetal forces matrix, $G(q) \in \mathbb{R}^n$ is the gravitational forces and torques vector, $F(\dot{q}) \in \mathbb{R}^n$ defines the drag forces vector, and $q \in \mathbb{R}^n$ defines the Cartesian position and orientation of the drone, and $u \in \mathbb{R}^n$ defines the thrust force and torques in the direction of the corresponding body frame angles. It is well known that the drone's dynamics can be linearly parametrized by the product of a vector of basis functions $\Phi = \Phi(q,\dot{q},u) \in \mathbb{R}^{p\times n}$ and a vector of parameters $\Theta \in \mathbb{R}^p$, where p is the number of parameters.

Remark 1: In contrast to other mechanical systems, the inertia matrix M of a drone is constant and hence the UAV model can be linearly parametrized as in (1).

Remark 2: The control input u stabilizes the drone's dynamics and guarantee trajectory tracking [33]. Here it is assumed that the control gain and control structure is known in advance. The drone's controller has the following structure $u = Kf(\widetilde{q})$, where $K \in \mathbb{R}^{n\times n}$ denotes a matrix gain and $\widetilde{q} = q^d - q \in \mathbb{R}^n$ is the error between the drone's states q and a desired reference $q^d \in \mathbb{R}^n$ and $f(\cdot) \in \mathbb{R}^n$ is a function of the error and its derivatives.

Consider an estimated model of the drone's dynamics of the form

$$\ddot{w} = \widehat{M}^{-1}[v - \widehat{C}(w,\dot{w})\dot{w} - \widehat{F}(\dot{w}) - \widehat{G}(w)] = \Phi_w^\top\widehat{\Theta} \quad (2)$$

where $w \in \mathbb{R}^n$ denotes the states of the estimated model, $v \in \mathbb{R}^m$ is the control input which has the same structure as u; the terms $\widehat{M} \in \mathbb{R}^{n\times n}$, $\widehat{C} \in \mathbb{R}^{n\times n}$, $\widehat{F} \in \mathbb{R}^n$, and $\widehat{G} \in \mathbb{R}^n$ are estimates of the inertia, Coriolis, drag forces, and gravitational matrices, respectively. The drone's estimated model is linearly parametrized by a set of basis functions $\Phi_w = \Phi(w,\dot{w},v) \in \mathbb{R}^{p\times n}$ and a vector of parameter estimates $\widehat{\Theta} \in \mathbb{R}^p$ of Θ. The control input v is defined as $v = Kf(\widetilde{w})$, where $\widetilde{w} = q^d - w$ defines the error between the desired reference q^d and the estimated model states w. Here the control gain K is the same as control u. Define the output error between the drone's dynamics and the estimated model as $e := q - w$.

The difference between the basis functions can be equivalently written as $(\Phi - \Phi_w)^\top\Theta = \varepsilon$, where ε defines a bounded approximation error, i.e., $\|\varepsilon\| \leq \bar{\varepsilon}$ with $\bar{\varepsilon} > 0$. Without loss of generality, we can express the approximation error as $\varepsilon = -K_1 e - K_2\dot{e} + \varepsilon_w$, where $K_1, K_2 > 0$ are positive definite matrices and $\varepsilon_w = \varepsilon + K_1 e + K_2\dot{e} \in \mathbb{R}^n$ denotes a bounded approximation error, i.e., $\|\varepsilon_w\| \leq \bar{\varepsilon}_w > 0$, which is a valid assumption since the basis functions are assumed to be Lipschitz [34].

The error dynamics between (1) and (2) is

$$\begin{aligned}\ddot{e} =& \ddot{q} - \ddot{w} = \Phi^\top\Theta - \Phi_w^\top\widehat{\Theta} \\ =& -K_1 e - K_2\dot{e} - \Phi_w^\top\widetilde{\Theta} + \varepsilon_w. \end{aligned} \quad (3)$$

Parameter estimates convergence can guaranteed if the vector of basis functions Φ_w fulfils the following lemma

Lemma 1: [35] The vector $\Phi_w \in \mathbb{R}^{p\times n}$ is said to be persistent exciting (PE) in the interval $[t : t+T]$ if there exists constants $\beta_0, \beta_1, T > 0$ that verifies

$$\beta_0 I \leq S = \int_t^{t+T} \Phi_w\Phi_w^\top d\tau \leq \beta_1 I \quad (4)$$

To fulfil lemma 1, it is assumed that a known excitation signal $\eta \in \mathbb{R}$ is added in the control inputs u and v. The following theorem establishes the uniform ultimate boundedness (UUB) [36] of the parametric error $\widetilde{\Theta}$ if the basis functions vector Φ_w fulfil the PE condition (4).

Theorem 1: Consider the error dynamics (3). Assume that the vector of basis functions Φ_w fulfils the PE condition (4). If the parameters $\widehat{\Theta}$ are updated as

$$\dot{\widetilde{\Theta}} = \dot{\widehat{\Theta}} = \Gamma\Phi_w(e + \dot{e}), \quad (5)$$

where $\Gamma \in \mathbb{R}^{p\times p}$ is a positive definite matrix; and $K_2 - I > 0$ then, there exists a bound

$$\alpha = \min\{\lambda_{\min}(K_2 - I), \lambda_{\min}(K_1)\} \quad (6)$$

that satisfies

$$\alpha > \sqrt{2}\bar{\varepsilon}_w + \rho, \quad (7)$$

for any $\rho > 0$. Then the error dynamics (3) are UUB with a practical bound $\mu_1 = \frac{\sqrt{2}\bar{\varepsilon}_w}{\alpha}$ and the parameter estimates $\widehat{\Theta}$ remain bounded.

An additional result of linear-time variant (LTV) systems is required for Theorem 1 proof. The result is stated in the next lemma

Lemma 2: [37] Consider the update rule (5) with output defined as the following linear-time varying (LTV) system

$$\begin{aligned} \dot{\widetilde{\Theta}} &= \Gamma\Phi_w(e+\dot{e}) \\ y &= \Phi_w^\top\widetilde{\Theta} \end{aligned} \tag{8}$$

then, the PE condition (4) is equivalent to the uniform complete observability (UCO) of system (8) and hence, boundedness of $\widetilde{\Theta}$ can be concluded.

Proof: The LTV system (8) and the system defined by $\dot{\widetilde{\Theta}} = \Gamma\Phi_w\nu$, $y = \Phi_w^\top\widetilde{\Theta}$ are equivalent under the control feedback $\nu = e + \dot{e}$ and therefore, by the UCO lemma, the state $\widetilde{\Theta}$ remain bounded. This completes the proof. ∎

With the above result we can proceed to prove Theorem 1. *Proof:* Consider the following Lyapunov function

$$V = \frac{1}{2}\dot{e}^\top\dot{e} + \frac{1}{2}\widetilde{\Theta}^\top\Gamma^{-1}\widetilde{\Theta} + \frac{1}{2}e^\top(K_1+K_2)e + e^\top\dot{e}. \tag{9}$$

It is easy to verify that the Lyapunov function (9) is positive definite by rewriting V as

$$V = \frac{1}{2}\begin{bmatrix} e \\ \dot{e} \end{bmatrix}^\top \begin{bmatrix} K_1+K_2 & I \\ I & I \end{bmatrix} \begin{bmatrix} e \\ \dot{e} \end{bmatrix} + \frac{1}{2}\widetilde{\Theta}^\top\Gamma^{-1}\widetilde{\Theta}, \tag{10}$$

which is positive definite if $K_1+K_2-I>0$ or, more strictly, if $K_2 - I > 0$. This condition is easy to verify by increasing the approximation error ε_w which does not violate the final result.

The time-derivative of V along the error dynamics trajectories (3) and the update rule (5) gives

$$\begin{aligned} \dot{V} =& -\dot{e}^\top(K_2-I)\dot{e} + (e+\dot{e})^\top\varepsilon_w - e^\top K_1 e \\ \leq& -\lambda_{\min}(K_2-I)\|\dot{e}\|^2 - \lambda_{\min}(K_1)\|e\|^2 \\ &+ \|\varepsilon_w\|(\|e\|+\|\dot{e}\|). \end{aligned}$$

Define $E = [\|e\|, \|\dot{e}\|]^\top$ and $\delta = [1,1]^\top$, then

$$\begin{aligned} \dot{V} \leq& -\alpha\|E\|^2 + E^\top\delta\|\varepsilon_w\| \\ \leq& -\alpha\|E\|^2 + \sqrt{2}\|E\|\bar{\varepsilon}_w = -\alpha\|E\|\left(\|E\| - \frac{\sqrt{2}\bar{\varepsilon}_w}{\alpha}\right). \end{aligned} \tag{11}$$

$\dot{V}$ is negative definite if $\|E\| > \frac{\sqrt{2}\bar{\varepsilon}_w}{\alpha} \equiv \mu_1$. Then, if the vector of basis functions Φ_w is PE, then the error vector E converges into a bounded set S_μ of radius μ_1 and the trajectories of (3) are UUB. Moreover, since E is bounded then it implies that w, $\dot{w}$, and Φ_w are also bounded and hence,

$$y \equiv \varepsilon_w - \ddot{e} - K_1 e - K_2\dot{e}, \tag{12}$$

is also bounded. Applying Lemma 2 allows to conclude that boundedness of E and y ensures boundedness of the parametric error $\widetilde{\Theta}$ and consequently of $\widehat{\Theta}$. This completes the proof. ∎

Fig. 1 depicts the general scheme of the proposed CLOE physics parameterization diagram. Here, we can observe clearly how both the states and parameters are estimated simultaneously using the identification law and the estimated model. This approach deals directly with a linear parameterization of the drone's dynamics which guarantees UUB solutions. However, notice that α cannot be adjusted since

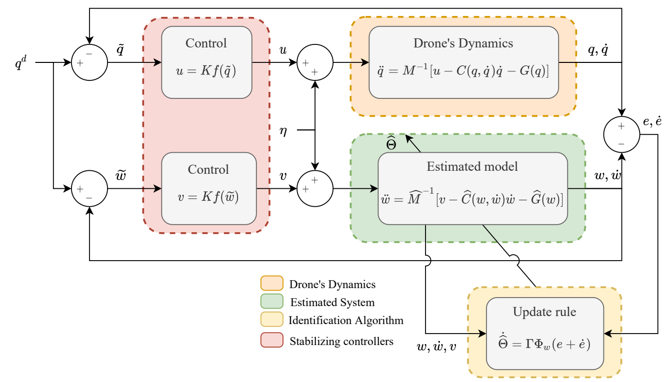

Fig. 1. CLOE Physics Parameterization Diagram

K_1 and K_2 are unknown. Furthermore, if K_1 and K_2 are increased then the approximation error ε_w is also increased. In the next section, a different parameterization based on the solution of the drone's differential equation is proposed that incorporates an admittance-type filter as hyperparameter that admits a certain amount of information of the basis function vector for the inference/identification task

III. Closed-Loop Output Error Approach: An Admittance Parameterization

The drone's dynamics (1) can be equivalently written as

$$\ddot{q} = -K_a q - B_a\dot{q} + K_a q + B_a\dot{q} + \Phi^\top\Theta. \tag{13}$$

where $K_a, B_a \in \mathbb{R}^{n\times n}$ denote a stiffness and damping matrices related to a virtual admittance model [38]. Assume the admittance gains are designed to fulfil the following equalities

$$\begin{aligned} K_a &= \Lambda_1\Lambda_2 \\ B_a &= \Lambda_1 + \Lambda_2, \end{aligned} \tag{14}$$

for some $\Lambda_1, \Lambda_2 > 0 \in \mathbb{R}^{n\times n}$ and $\Lambda_1 \neq \Lambda_2$. The Laplace transform of the differential equation (13) is

$$\begin{aligned} Q(s) =& \; Z^{-1}(s)\dot{q}(t_0) + Z^{-1}(s)[sI + Ba]q(t_0) \\ &+ Z^{-1}(s)\mathcal{L}\left\{B_a\dot{q} + K_a q + \Phi^\top\Theta\right\} \end{aligned} \tag{15}$$

where $Z(s) = s^2 I + sB_a + K_a$ is equivalent to an admittance filter. The following theorem establishes the state parameterization of the solution of (13) which will be used for the inference/identification problem [39].

Theorem 2: Assume the admittance parameters B_a and K_a satisfies (14). The solution of the drone's differential equation (1) under the admittance filter $Z(s) = s^2 I + B_a s + K_a$ is

$$\begin{aligned} q(t) =& \; A\left(\Lambda_2 e^{-\Lambda_1(t-t_0)} - \Lambda_1 e^{-\Lambda_2(t-t_0)}\right)q(t_0) \\ &+ A\left(e^{-\Lambda_1(t-t_0)} - e^{-\Lambda_2(t-t_0)}\right)\dot{q}(t_0) \\ &+ AL(q,\dot{q}) + AH(q,\dot{q})\Theta, \end{aligned} \tag{16}$$

for some filter functions $L(\cdot) \in \mathbb{R}^n$ and $H(\cdot) \in \mathbb{R}^{n\times p}$. The terms $A, \Lambda_1, \Lambda_2 \in \mathbb{R}^{n\times n}$ are functions dependent on the admittance gains K_a and B_a.

Proof: First, consider the first element of the right-hand side of (15)

$$Q^1(s) = (s^2 I + B_a s + K_a)^{-1}\dot{q}(t_0).$$

Using partial fractions gives

$$\begin{aligned}Q^1(s) &= [(sI+\Lambda_1)(sI+\Lambda_2)]^{-1}\dot q(t_0)\\ &= A\left((sI+\Lambda_1)^{-1}-(sI+\Lambda_2)^{-1}\right)\dot q(t_0)\\ q^1(t) &= A\left(e^{-\Lambda_1(t-t_0)}-e^{-\Lambda_2(t-t_0)}\right)\dot q(t_0)\end{aligned}$$

where $A=(\Lambda_2-\Lambda_1)^{-1}$. Following a similar procedure for the second element of (15) gives

$$\begin{aligned}Q^2(s) &= \left((sI+\Lambda_1)(sI+\Lambda_2)\right)^{-1}(sI+Ba)\,q(t_0)\\ &= \left(C_1(sI+\Lambda_1)^{-1}+C_2(sI+\Lambda_2)^{-1}\right)q(t_0)\\ q^2(t) &= \left(C_1e^{-\Lambda_1(t-t_0)}+C_2e^{-\Lambda_2(t-t_0)}\right)q(t_0).\end{aligned}$$

where $C_1=A\Lambda_2$ and $C_2=-A\Lambda_1$.

For the third part of (15), we have that

$$Q^3(s)=(s^2I+B_as+K_a)^{-1}\mathcal{L}\left\{B_a\dot q+K_aq+\Phi^\top\Theta\right\}$$

whose solution verifies the following convolution integral

$$\begin{aligned}q^3(t)=&A\int_{t_0}^t(e^{-\Lambda_1(t-\tau)}-e^{-\Lambda_2(t-\tau)})(B_a\dot q+K_pq)d\tau\\ &+A\int_{t_0}^t(e^{-\Lambda_1(t-\tau)}-e^{-\Lambda_2(t-\tau)})\Phi^\top(q,\dot q,u)d\tau\cdot\Theta\end{aligned}$$

Define

$$\begin{aligned}l_i(q,\dot q)&=\int_{t_0}^t e^{-\Lambda_i(t-\tau)}(B_a\dot q+K_aq)d\tau\in\mathbb{R}^n\\ h_i(q,\dot q)&=\int_{t_0}^t e^{-\Lambda_i(t-\tau)}\Phi^\top(q,\dot q,u)d\tau\in\mathbb{R}^{n\times p},\quad i=1,2.\end{aligned}$$

The above definitions can be easily computed using the following low-pass filters

$$\dot l_i(q,\dot q)=-\Lambda_il_i(q,\dot q)+B_a\dot q+K_aq, \tag{17a}$$
$$\dot h_i(q,\dot q)=-\Lambda_ih_i(q,\dot q)+\Phi^\top(q,\dot q,u),\quad i=1,2. \tag{17b}$$

Therefore, the state parameterization of the solution of (1) is given by

$$\begin{aligned}q(t)=&q^1(t)+q^2(t)+q^3(t)\\ =&A\left(e^{-\Lambda_1(t-t_0)}-e^{-\Lambda_2(t-t_0)}\right)\dot q(t_0)\\ &+A\left(\Lambda_2e^{-\Lambda_1(t-t_0)}-\Lambda_1e^{-\Lambda_2(t-t_0)}\right)q(t_0)\\ &+AL(q,\dot q)+AH(q,\dot q)\Theta\end{aligned}\tag{18}$$

where $L(q,\dot q)=[l_1(q,\dot q)-l_2(q,\dot q)]\in\mathbb{R}^n$ and $H(q,\dot q)=[h_1(q,\dot q)-h_2(q,\dot q)]\in\mathbb{R}^{n\times p}$. This completes the proof. ■

The filters associated to the basis functions $h_1(\cdot)$ and $h_2(\cdot)$ verifies the following bounds

$$\begin{aligned}\|h_1(q,\dot q)\|&\le\int_{t_0}^t\|e^{-\Lambda_1(t-\tau)}\|\cdot\|\Phi^\top\|d\tau\\ &\le\left(\int_{t_0}^te^{-2\lambda_1(t-\tau)}d\tau\right)^{\frac12}\left(\int_{t_0}^t\Phi\Phi^\top d\tau\right)^{\frac12},\\ \|h_2(q,\dot q)\|&\le\int_{t_0}^t\|e^{-\Lambda_2(t-\tau)}\|\cdot\|\Phi^\top\|d\tau\\ &\le\left(\int_{t_0}^te^{-2\lambda_2(t-\tau)}d\tau\right)^{\frac12}\left(\int_{t_0}^t\Phi\Phi^\top d\tau\right)^{\frac12}.\end{aligned}$$

Notice that we obtain almost the same PE condition (4), where the integral can be written as a sum of $N=\frac{t-T-t_0}{T}$ time windows as

$$\int_{t_0}^t\Phi\Phi^\top d\tau=\sum_{\kappa=0}^N\int_a^{a+T}\Phi\Phi^\top d\tau,$$

where $a=t_0+\kappa T$. So, the filters are bounded by

$$\sqrt{\frac{\beta_0N}{2\lambda_1}}\le\|h_i(q,\dot q)\|\le\sqrt{\frac{\beta_1N}{2\lambda_1}},\ i=1,2. \tag{19}$$

The solution of the estimated model (2) has the same structure as in (18)

$$\begin{aligned}w(t)=&A\left(e^{-\Lambda_1(t-t_0)}-e^{-\Lambda_2(t-t_0)}\right)\dot q(t_0)\\ &+A\left(\Lambda_2e^{-\Lambda_1(t-t_0)}-\Lambda_1e^{-\Lambda_2(t-t_0)}\right)q(t_0)\\ &+AL(w,\dot w)+AH(w,\dot w)\widehat\Theta.\end{aligned}\tag{20}$$

The identification error between (18) and (20) is

$$e=q-w=-AH(w,\dot w)\widetilde\Theta+A\varepsilon_h \tag{21}$$

where $\varepsilon_h=[L(q,\dot q)-L(w,\dot w)]+[H(q,\dot q)-H(w,\dot w)]\Theta\in\mathbb{R}^n$ is an approximation error associated to each filter. The next theorem establishes the UUB of the parametric error $\widetilde\Theta$ and identification error e trajectories as long as the PE condition (4) is satisfied.

Theorem 3: Consider the trajectories of the identification error solution (21). If the parameter estimates are updated by

$$\dot{\widetilde\Theta}=\dot{\widehat\Theta}=\Gamma H^\top(w,\dot w)Ae \tag{22}$$

and the vector of basis functions Φ_w fulfils the PE condition (4), then the trajectories of (21) are UUB with a practical bound $\mu_3=\left(\frac{\lambda^2_{\max}(H)}{\lambda^2_{\min}(H)}+1\right)\bar\varepsilon_h$ and the parameter estimates $\widehat\Theta$ remain bounded in a set S_Θ of radius $\mu_2=\frac{\lambda_{\max}(H)}{\lambda^2_{\min}(H)}\bar\varepsilon_h$.

Proof: Consider the following Lyapunov function

$$W=\frac12\widetilde\Theta^\top\Gamma^{-1}\widetilde\Theta. \tag{23}$$

The time-derivative of W under the update rule (22) and identification error (21) gives

$$\begin{aligned}\dot W=&\widetilde\Theta^\top H^\top(w,\dot w)A^\top e\\ =&-\widetilde\Theta^\top H^\top(w,\dot w)A^2H(w,\dot w)\widetilde\Theta+\widetilde\Theta^\top H^\top(w,\dot w)A^2\varepsilon_h\\ \le&-k_a^2\lambda^2_{\min}(H)\|\widetilde\Theta\|^2+k_a^2\lambda_{\max}(H)\|\varepsilon_h\|\|\widetilde\Theta\|,\end{aligned}$$

where $\|A\|=k_a>0$. $\dot V$ is negative definite if

$$\|\widetilde\Theta\|>\frac{\lambda_{\max}(H)}{\lambda^2_{\min}(H)}\bar\varepsilon_h\equiv\mu_2.$$

If the basis functions within $H(w,\dot w)$ fulfil the PE condition (4) then, the parametric error $\widetilde\Theta$ converges to a bounded set S_Θ of radius μ_2, that is, $\|\widetilde\Theta\|\le\mu_2$ and hence, the parametric error $\widetilde\Theta$ remain bounded. With this result is easy to verify that the identification error is bounded by

$$\begin{aligned}\|e\|&\le k_a\|H(w,\dot w)\|\|\widetilde\Theta\|+k_a\|\varepsilon_h\|\\ &\le\left(\frac{\lambda^2_{\max}(H)}{\lambda^2_{\min}(H)}+1\right)k_a\bar\varepsilon_h.\end{aligned}$$

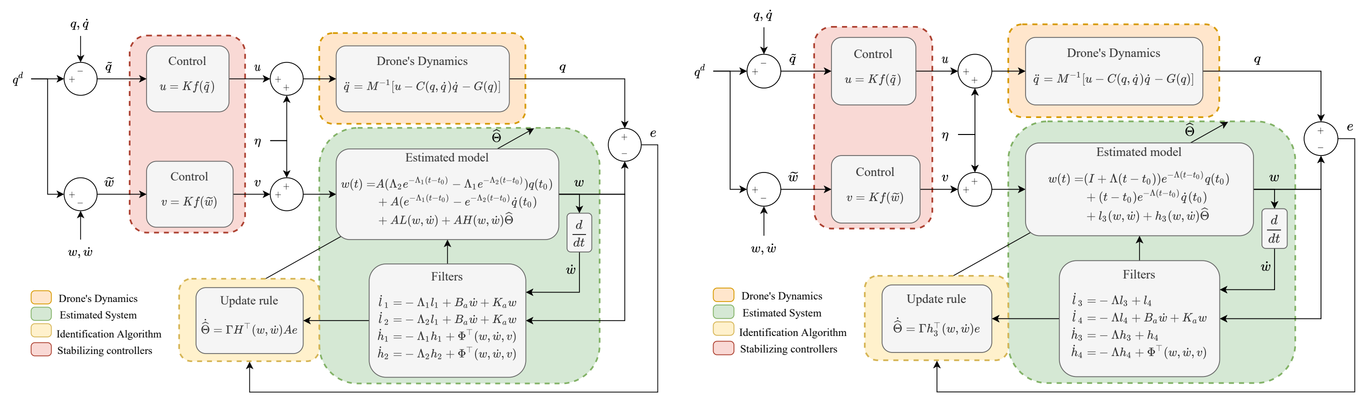

(a) An Admittance Parameterization

(b) A Nested Admittance Parameterization

Fig. 2. CLOE Admittance Parameterization diagrams

The above result relates directly the identification error e and the approximation error ε_h. In addition, the update rule (22) fulfils Lemma 2 by considering the LTV system

$$
\begin{aligned}
\dot{\widetilde{\Theta}} &= \Gamma H^\top(w,\dot{w})A\nu \\
\zeta &= AH(w,\dot{w})\widetilde{\Theta} \equiv A\varepsilon_h - e
\end{aligned}
$$

under the control input $\nu = e$. Using the UCO lemma allows concluding that boundedness of e and ζ implies boundedness of the parametric error $\widetilde{\Theta}$ and hence $\widehat{\Theta}$ is also bounded. This completes the proof. ∎

IV. Closed-Loop Output Error: A Nested Admittance Parameterization

In the previous section we design a CLOE algorithm based on an admittance parameterization when only partial measurements of the states are available. The approach assumes that the parameters of the filter are based on two design parameters Λ_1 and Λ_2. In this section we simplify the approach by using a nested admittance model that only requires one design parameter Λ. In this scenario, the admittance parameters verify

$$
K_a \;= \Lambda^2, \quad B_a = 2\Lambda, \tag{24}
$$

for any $\Lambda > 0 \in \mathbb{R}^{n\times n}$. The following theorem establishes the state parameterization of the solution of (13) under the admittance parameters assumption (24).

Theorem 4: Assume the admittance parameters verify (24). The solution of the drone's differential equation (1) under the admittance filter $Z(s) = s^2I + B_a s + K_a$ is

$$
\begin{aligned}
q(t) = \;& (I+\Lambda(t-t_0))e^{-\Lambda(t-t_0)}q(t_0) \\
&+ (t-t_0)e^{-\Lambda(t-t_0)}\dot{q}(t_0) + l_3(q,\dot{q}) + h_3(q,\dot{q})\Theta,
\end{aligned} \tag{25}
$$

for some filter functions $l_3(\cdot) \in \mathbb{R}^n$ and $h_3(\cdot) \in \mathbb{R}^{n\times p}$.

Proof: First, consider the first element of the right-hand side of (15). Using partial fractions gives

$$
\begin{aligned}
Q^1(s) &= (s^2I + B_a s + K_a)^{-1}\dot{q}(t_0), \\
Q^1(s) &= (sI+\Lambda)^{-2}\dot{q}(t_0) \\
q^1(t) &= (t-t_0)e^{-\Lambda(t-t_0)}\dot{q}(t_0).
\end{aligned}
$$

Following a similar procedure for the second element of (15) gives

$$
\begin{aligned}
Q^2(s) &= (sI+\Lambda)^{-2}(sI+Ba)\,q(t_0) \\
&= \left((sI+\Lambda)^{-1} + \Lambda(sI+\Lambda)^{-2}\right)q(t_0) \\
q^2(t) &= (I+\Lambda(t-t_0))\,e^{-\Lambda(t-t_0)}q(t_0).
\end{aligned}
$$

For the third part of (15), we have that

$$
Q^3(s) = (s^2I + B_a s + K_a)^{-1}\mathcal{L}\left\{B_a\dot{q} + K_a q + \Phi^\top\Theta\right\}
$$

whose solution verifies the following convolution integral

$$
\begin{aligned}
q^3(t) = &\int_{t_0}^{t}(t-\tau)e^{-\Lambda(t-\tau)}(B_a\dot{q} + K_a q)d\tau \\
&+ \int_{t_0}^{t}(t-\tau)e^{-\Lambda(t-\tau)}\Phi^\top(q,\dot{q},u)d\tau\cdot\Theta.
\end{aligned}
$$

The following low-pass filters are defined

$$
\begin{aligned}
\dot{l}_3(q,\dot{q}) &= -\Lambda l_3(q,\dot{q}) + l_4(q,\dot{q}), && \text{(26a)}\\
\dot{l}_4(q,\dot{q}) &= -\Lambda l_4(q,\dot{q}) + B_a\dot{q} + K_a q && \text{(26b)}\\
\dot{h}_3(q,\dot{q}) &= -\Lambda h_3(q,\dot{q}) + h_4(q,\dot{q}), && \text{(26c)}\\
\dot{h}_4(q,\dot{q}) &= -\Lambda h_4(q,\dot{q}) + \Phi^\top(q,\dot{q},u) && \text{(26d)}
\end{aligned}
$$

Therefore, the state parameterization of the solution of (1) is given by

$$
\begin{aligned}
q(t) =& q^1(t) + q^2(t) + q^3(t) \\
&= (I+\Lambda(t-t_0))\,e^{-\Lambda(t-t_0)}q(t_0) \\
&\quad + (t-t_0)e^{-\Lambda(t-t_0)}\dot{q}(t_0) + l_3(q,\dot{q}) + h_3(q,\dot{q})\Theta
\end{aligned} \tag{27}
$$

This completes the proof. ∎

The diagrams of the admittance parameterizations are depicted in Fig. 2. The results of Theorem 4 hold for this parameterization and the update rule is slightly modified to

$$
\dot{\widetilde{\Theta}} = \dot{\widehat{\Theta}} = \Gamma h_3^\top(w,\dot{w})e. \tag{28}
$$

V. Simulation studies

In this section, we test the proposed inference algorithms using a quadcopter model. The quadcopter satisfies the following dynamic model

$$\begin{bmatrix}\ddot{x}\\ \ddot{y}\\ \ddot{z}\end{bmatrix} = \frac{F}{m}\begin{bmatrix}c_\psi s_\theta c_\phi + s_\psi s_\phi\\ s_\psi s_\theta c_\phi - c_\psi s_\phi\\ c_\theta c_\phi\end{bmatrix} - \frac{1}{m}\begin{bmatrix}A_x\dot{x}\\ A_y\dot{y}\\ A_z\dot{z}\end{bmatrix} - \begin{bmatrix}0\\0\\g\end{bmatrix}$$

$$\begin{bmatrix}\ddot{\phi}\\ \ddot{\theta}\\ \ddot{\psi}\end{bmatrix} = \begin{bmatrix}\frac{1}{I_{xx}}\tau_\phi\\ \frac{1}{I_{yy}}\tau_\theta\\ \frac{1}{I_{zz}}\tau_\psi\end{bmatrix} - \begin{bmatrix}\frac{I_{yy}-I_{zz}}{I_{xx}}\dot{\theta}\dot{\psi}\\ \frac{I_{zz}-I_{xx}}{I_{yy}}\dot{\phi}\dot{\psi}\\ \frac{I_{xx}-I_{yy}}{I_{zz}}\dot{\phi}\dot{\theta}\end{bmatrix}$$

where x, y, z denote the pose and ϕ, θ, ψ denote the orientation of the drone, m is the mass of the quadcopter, I_{xx}, I_{yy}, I_{zz} are the moments of inertia, A_x, A_y, A_z are the drag forces, g is the gravitational acceleration, F is thrust force, τ_ϕ, τ_θ, and τ_ψ are the roll, pitch, and yaw torques. The complete state vector is $q = [x, y, z, \phi, \theta, \psi]^\top \in \mathbb{R}^6$ and $u = [F, \tau_x, \tau_y, \tau_z]^\top \in \mathbb{R}^4$.

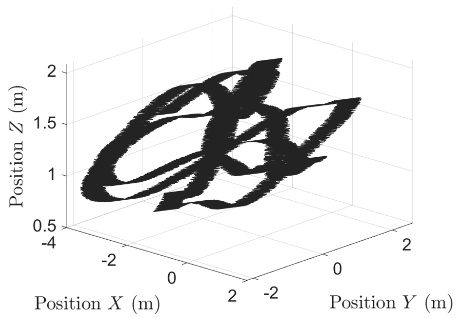

(a) Noisy-measured trajectory

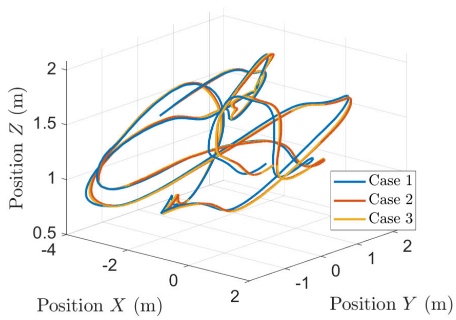

(b) Estimated trajectory

Fig. 3. Trajectory Inference results

In these experiments we adopt a control tracking formulation which divides the control input u into a position and orientation controller. The position control calculates the total thrust F and the desired roll ϕ^d and yaw θ^d angles as

$$\begin{aligned}\phi^d &= \arcsin\left(\frac{r_x s_\psi - r_y c_\psi}{\sqrt{r_x^2 + r_y^2 + (r_z+g)^2}}\right),\\ \theta^d &= \arctan\left(\frac{r_x c_\psi + r_y s_\psi}{r_z + g}\right),\\ F &= r_x(s_\theta c_\psi c_\phi + s_\psi s_\phi) + r_y(s_\theta s_\psi c_\phi - c_\psi s_\phi)\\ &\quad + (r_z+g)c_\theta c_\phi,\end{aligned}$$

where the command references r_x, r_y, and r_z are computed with the following PD control structures $r_x = \ddot{x}^d + k_{dx}\dot{e}_x + k_{px}e_x,\ r_y = \ddot{y}^d + k_{dy}\dot{e}_y + k_{py}e_y,\ r_z = \ddot{z}^d + k_{dz}\dot{e}_z + k_{pz}e_z$, where $k_{pi} > 0$ and $k_{di} > 0$ are the proportional and derivative gains in the $i = x, y, z$ directions. The position errors are defined as $e_x = x^d - x,\ e_y = y^d - y,\ e_z = z^d - z$, for some desired references $x^d, y^d, z^d \in \mathbb{R}$. The orientation control has the same PD structure and is given by $\tau_\phi = \ddot{\phi}^d + k_{d\phi}\dot{e}_\phi + k_{p\phi}e_\phi,\ \tau_\theta = \ddot{\theta}^d + k_{d\theta}\dot{e}_\theta + k_{p\theta}e_\theta,\ \tau_\psi = \ddot{\psi}^d + k_{d\psi}\dot{e}_\psi + k_{p\psi}e_\psi$, where $k_{pj}, k_{dj} > 0$ denotes the proportional and derivative gains of the roll, pitch and yaw directions $j = \phi, \theta, \psi$. The orientation errors are defined as $e_\phi = \phi^d - \phi,\ e_\theta = \theta^d - \theta,\ e_\psi = \psi^d - \psi$, where ϕ^d and θ^d are computed by the position controller, and ψ^d can be defined by the user.

Assume that the drag forces coefficients are the same, that is, $A_x = A_y = A_z$. The parameters to estimate are: $\theta_1 = \frac{1}{m}$, $\theta_2 = \frac{A_x}{m}$, $\theta_3 = \frac{1}{I_{xx}}$, $\theta_4 = \frac{1}{I_{yy}}$, $\theta_5 = \frac{1}{I_{zz}}$, $\theta_6 = \frac{I_{yy}-I_{zz}}{I_{xx}}$, $\theta_7 = \frac{I_{zz}-I_{xx}}{I_{yy}}$, $\theta_8 = \frac{I_{xx}-I_{yy}}{I_{zz}}$, and $\theta_9 = g$.

The PD control gains obtained in [40] are used as stabilization gains. The reported gains are: $k_{px} = k_{py} = k_{pz} = 0.7071$, $k_{dx} = k_{dy} = k_{dz} = 1.3836$, $k_{p\phi} = k_{p\theta} = k_{p\psi} = 1.8597$, and $k_{d\phi} = k_{d\theta} = k_{d\psi} = 6.9177$. The desired position references are given by $r_x = -2 + 2\cos\left(\frac{2\pi}{20}t\right),\ r_y = 2\sin\left(\frac{2\pi}{20}t\right),\ r_z = \frac{3}{30^2}t^2 - \frac{2}{30^3}t^3$ if $t < 30$, otherwise $r_z = 1$.

Three different cases are considered: i) Case 1: CLOE with physics parameterization, ii) Case 2: CLOE with admittance parameterization, and iii) Case 3: CLOE with nested admittance parameterization. The update rule and filter gains are manually tuned until the best inference results are obtained. The final gains are given in Table I.

TABLE I
Update rule and Filters Gains

Case	Γ	Λ_1	Λ_2
Case 1	diag{ 20, 20, 2000, 2000, 2000, 20, 20, 20, 20}	-	-
Case 2	diag{ 20, 20, 4000, 4000, 4000, 20, 20, 20, 2000}	$20I_6$	$2I_6$
Case 3	diag{ 20, 20, 4000, 4000, 4000, 20, 20, 20, 2000}	diag{ 5, 5, 5, 100, 100, 100}	

Fig. 3 depicts the trajectory inference results. The first plot shows the noisy-trajectory from sensors measurements. The second plot shows the estimated trajectory that exhibits noise attenuation and a smooth performance.

TABLE II
Parameter estimates of the quadcopter through the Physics update rule (5) and the Admittance update rule (22)

Estimate $\widehat{\Theta}_k$	Real value Θ_k	CLOE Algorithm					
		Case 1	$\lvert\widetilde{\Theta}_k\rvert$ (%)	Case 2	$\lvert\widetilde{\Theta}_k\rvert$ (%)	Case 3	$\lvert\widetilde{\Theta}_k\rvert$ (%)
$\widehat{\theta}_1$	1.7857	1.7884	0.1495	2.2918	28.341	2.2253	24.6164
$\widehat{\theta}_2$	0.1786	0.1779	0.3912	-0.2201	223.2421	-0.1783	199.8497
$\widehat{\theta}_3$	70.4225	70.3938	0.0407	42.0474	40.2926	41.1249	41.6025
$\widehat{\theta}_4$	70.4225	70.421	0.0021	44.2255	37.1998	115.7439	64.3564
$\widehat{\theta}_5$	35.2113	16.9372	51.8995	23.8476	32.273	8.0798	77.0534
$\widehat{\theta}_6$	-1	-2.2023	120.2264	0.1437	114.3702	0.1011	110.1078
$\widehat{\theta}_7$	1	3.7435	274.3494	0.1191	88.0926	0.0998	90.0159
$\widehat{\theta}_8$	0	-0.003	0.3	-0.002	0.2	0.087	8.7
$\widehat{\theta}_9$	9.81	9.8254	0.157	12.6004	28.4444	12.2338	24.7073

Fig. 4 shows the position and orientation inference results. Case 1 exhibits accurate results with noise attenuation for

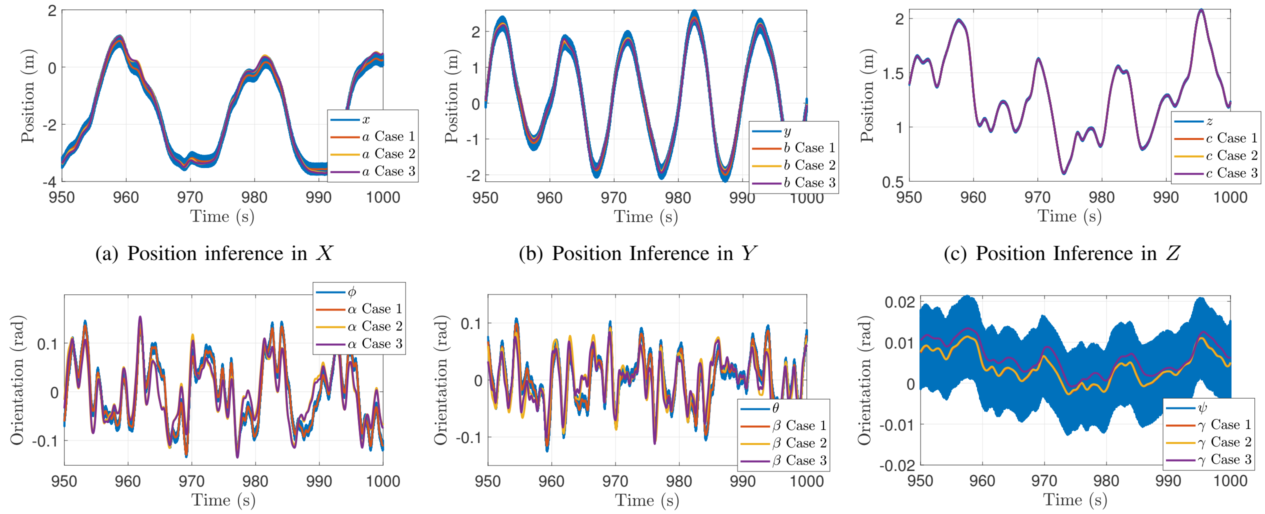

(a) Position inference in X (b) Position Inference in Y (c) Position Inference in Z

(d) Orientation inference in ϕ (e) Orientation inference in θ (f) Orientation inference in ψ

Fig. 4. Position and Orientation inference results

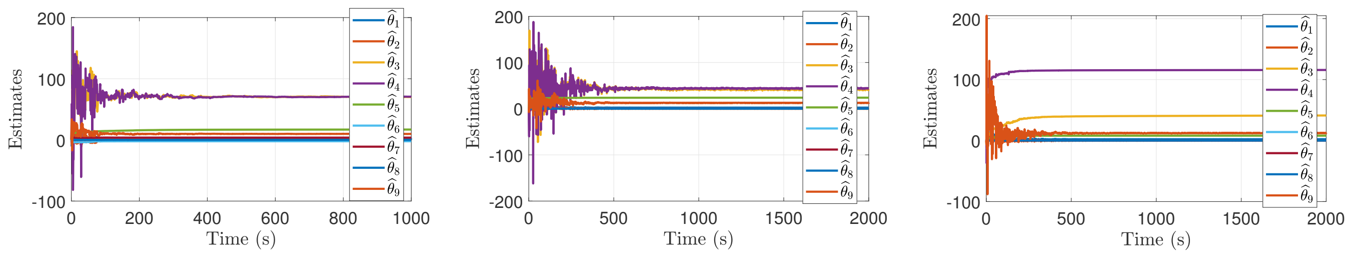

(a) CLOE: Physics Parameterization (b) CLOE: Admittance Parameterization with two filters (c) CLOE: Admittance Parameterization with nested filters

Fig. 5. Parameter estimates $\widehat{\Theta}$

both the position and orientation trajectories. On the other hand, Case 2 and Case 3 exhibits similar results in the position trajectories but in the orientation trajectories have a small bias due to the selection of the admittance parameters. Moreover, the velocity error at the update rule (5) improves the identification and inference results.

The mean absolute identification error $\bar{e} = \frac{1}{N}|e_i|, \quad i = 1, \cdots, 6$, is used as performance metric between the physics informed model states and the real states measurements. The numerical results are given in Table III. It is clear that Case 1 has better results since it incorporates a complete physics informed model for both identification and estimation. Case 2 and CASE 3 do not require measurements of the velocity to estimate the real trajectory with an acceptable estimation error, however the incorporation of the admittance parameters cause some delay and bias. This fact can be seen at the orientation results because the admittance parameters used for the position trajectory estimation are not necessarily useful for the orientation estimation. Therefore, both Case 2 and Case 3 need an accurate tuning of the admittance parameters to reduce the delay and bias in the inference results.

Table II shows the identification error results of the CLOE algorithm. The parameter estimates of Case 1 converges to almost their real values except to the parameters associated to the yaw angle since the trajectories cannot excite that axis due to the drone's configuration. Nevertheless, the parameter estimates are close to their real values with small parametric error percentage $|\widetilde{\Theta}_k|$. On the other hand, the parameter estimates of Case 2 and Case 3 do not converge to their real values since the algorithm estimates different parameters due to the incorporation of the admittance filter. However, the estimates obtained from the algorithm construct a physics informed model that is used for the trajectory inference algorithm. Fig. 5 shows the parameter estimates convergence for each case.

TABLE III
NUMERICAL RESULTS OF $\bar{e}$

$\bar{e}$	Case 1	Case 2	Case 3
e_1	0.0995	0.1376	0.1340
e_2	0.0996	0.1137	0.1091
e_3	0.0050	0.0050	0.0050
e_4	0.0051	0.0303	0.0280
e_5	0.0050	0.0175	0.0195
e_6	0.0050	0.0050	0.0053

VI. CONCLUSIONS

This work reports a drone's physics informed trajectory inference algorithm. The algorithm is based on a closed-loop output error technique that constructs a physics informed model for trajectory inference. Two different schemes based on a physics and admittance parameterizations are given in accordance to the available states measurements. Stability and convergence of the inference algorithms are assessed using Lyapunov stability theory. Simulation studies are carried out to verify the effectiveness of the approach. The results show further work opportunities for filtering tuning to enhance the accuracy results of the admittance parameterization.

Further work focuses on complementary algorithms for intent prediction using the proposed inference algorithm. The scope includes self-learning models for non-parametric basis functions inference and the analysis for time-varying parameters. In addition, the use of reinforcement learning architectures gives an interesting open challenge for intent extraction of drone's mission profile.

References

[1] A. Perrusquía and W. Guo, "A closed-loop output error approach for physics-informed trajectory inference using online data," *IEEE Transactions on Cybernetics*, 2022.

[2] J.-P. Yaacoub, H. Noura, O. Salman, and A. Chehab, "Security analysis of drones systems: Attacks, limitations, and recommendations," *Internet of Things*, vol. 11, p. 100218, 2020.

[3] S. R. Ganti and Y. Kim, "Implementation of detection and tracking mechanism for small uas," in *2016 International Conference on Unmanned Aircraft Systems (ICUAS)*. IEEE, 2016, pp. 1254–1260.

[4] E. Páli, K. Mathe, L. Tamas, and L. Buşoniu, "Railway track following with the ar. drone using vanishing point detection," in *2014 IEEE International Conference on Automation, Quality and Testing, Robotics*. IEEE, 2014, pp. 1–6.

[5] R. Stolkin, D. Rees, M. Talha, and I. Florescu, "Bayesian fusion of thermal and visible spectra camera data for region based tracking with rapid background adaptation," in *2012 IEEE International Conference on Multisensor Fusion and Integration for Intelligent Systems (MFI)*. IEEE, 2012, pp. 192–199.

[6] C. J. Li and H. Ling, "Synthetic aperture radar imaging using a small consumer drone," in *2015 IEEE international symposium on antennas and propagation & USNC/URSI national radio science meeting*. IEEE, 2015, pp. 685–686.

[7] S. A. A. Rizvi and Z. Lin, "Reinforcement learning-based linear quadratic regulation of continuous-time systems using dynamic output feedback," *IEEE transactions on cybernetics*, vol. 50, no. 11, pp. 4670–4679, 2019.

[8] E. Archer, I. M. Park, L. Buesing, J. Cunningham, and L. Paninski, "Black box variational inference for state space models," *arXiv preprint arXiv:1511.07367*, 2015.

[9] R. Corteso, J. Park, and O. Khatib, "Real-time adaptive control for haptic telemanipulation with kalman active observers," *IEEE Transactions on Robotics*, vol. 22, no. 5, pp. 987–999, 2006.

[10] C. Wang, H. Han, J. Wang, H. Yu, and D. Yang, "A robust extended kalman filter applied to ultrawideband positioning," *Mathematical Problems in Engineering*, vol. 2020, 2020.

[11] R. Rezaie and X. R. Li, "Destination-directed trajectory modeling, filtering, and prediction using conditionally markov sequences," *IEEE Transactions on Aerospace and Electronic Systems*, vol. 57, no. 2, pp. 820–833, 2020.

[12] A. Perrusquía and W. Yu, "Discrete-time $\mathcal{H}_2$ neural control using reinforcement learning," *IEEE Transactions on Neural Networks and Learning Systems*, 2020.

[13] L. B. White and F. Carravetta, "State-space realizations and optimal smoothing for gaussian generalized reciprocal processes," *IEEE Transactions on Automatic Control*, vol. 65, no. 1, pp. 389–396, 2019.

[14] P. Geragersian, I. Petrunin, W. Guo, and R. Grech, "An ins/gnss fusion architecture in gnss denied environment using gated recurrent unit," in *AIAA SCITECH 2022 Forum*, 2022, p. 1759.

[15] G. Revach, N. Shlezinger, X. Ni, A. L. Escoriza, R. J. van Sloun, and Y. C. Eldar, "Kalmannet: Neural network aided kalman filtering for partially known dynamics," *arXiv preprint arXiv:2107.10043*, 2021.

[16] R. Rezaie and X. R. Li, "Gaussian conditionally markov sequences: Modeling and characterization," *Automatica*, vol. 131, p. 109780, 2021.

[17] C. E. Rasmussen, "Gaussian processes in machine learning," in *Summer school on machine learning*. Springer, 2003, pp. 63–71.

[18] W. Gilpin, "Chaos as an interpretable benchmark for forecasting and data-driven modelling," *arXiv preprint arXiv:2110.05266*, 2021.

[19] J. Ramírez, W. Yu, and A. Perrusquía, "Model-free reinforcement learning from expert demonstrations: a survey," *Artificial Intelligence Review*, pp. 1–29, 2021.

[20] A. Perrusquía and W. Yu, "Neural $\mathcal{H}_2$ control using continuous-time reinforcement learning," *IEEE Transactions on Cybernetics*, vol. 52, no. 6, pp. 4485–4494, 2022.

[21] C. M. Legaard, T. Schranz, G. Schweiger, J. Drgoňa, B. Falay, C. Gomes, A. Iosifidis, M. Abkar, and P. G. Larsen, "Constructing neural network-based models for simulating dynamical systems," *arXiv preprint arXiv:2111.01495*, 2021.

[22] A. Perrusquía and W. Yu, "Identification and optimal control of nonlinear systems using recurrent neural networks and reinforcement learning: An overview," *Neurocomputing*, vol. 438, pp. 145–154, 2021.

[23] N. M. Gottschling, V. Antun, B. Adcock, and A. C. Hansen, "The troublesome kernel: why deep learning for inverse problems is typically unstable," *arXiv preprint arXiv:2001.01258*, 2020.

[24] O. Nelles, "Nonlinear dynamic system identification," in *Nonlinear System Identification*. Springer, 2020, pp. 831–891.

[25] A. Janot, P.-O. Vandanjon, and M. Gautier, "Identification of physical parameters and instrumental variables validation with two-stage least squares estimator," *IEEE Transactions on Control Systems Technology*, vol. 21, no. 4, pp. 1386–1393, 2012.

[26] S. Zeng and E. Fernandez, "Adaptive controller design and disturbance attenuation for sequantially interconnected SISO linear systems under noisy output measurements with partly measured disturbances," *2008 American Control Conference*, 2008.

[27] A. Perrusquía, R. Garrido, and W. Yu, "Stable robot manipulator parameter identification: A closed-loop input error approach," *Automatica*, vol. 141, p. 110294, 2022.

[28] M. Brunot, A. Janot, F. Carrillo, J. Cheong, and J.-P. Noël, "Output error methods for robot identification," *Journal of Dynamic Systems, Measurement, and Control*, vol. 142, no. 3, 2020.

[29] A. Janot, M. Gautier, A. Jubien, and P. O. Vandanjon, "Comparison between the cloe method and the didim method for robots identification," *IEEE Transactions on Control Systems Technology*, vol. 22, no. 5, pp. 1935–1941, 2014.

[30] C. Urrea and J. Pascal, "Design and validation of a dynamic parameter identification model for industrial manipulator robots," *Archive of Applied Mechanics*, pp. 1–27, 2021.

[31] R. Garrido and R. Miranda, "DC servomechanism parameter identification: A closed loop input error approach," *ISA Transactions*, vol. 51, pp. 42–49, 2012.

[32] A. Perrusquía, R. Garrido, and W. Yu, "An input error method for parameter identification of a class of euler-lagrange systems," in *2021 18th International Conference on Electrical Engineering, Computing Science and Automatic Control (CCE)*. IEEE, 2021, pp. 1–6.

[33] A. Perrusquía and W. Yu, "Robust control under worst-case uncertainty for unknown nonlinear systems using modified reinforcement learning," *International Journal of Robust and Nonlinear Control*, vol. 30, no. 7, pp. 2920–2936, 2020.

[34] X. Xu, L. Liu, and G. Feng, "On lipschitz conditions of infinite dimensional systems," *Automatica*, vol. 117, p. 108947, 2020.

[35] A. Perrusquía, W. Yu, and X. Li, "Nonlinear control using human behavior learning," *Information Sciences*, vol. 569, pp. 358–375, 2021.

[36] F. Lewis, S. Jagannathan, and A. Yeşildirek, *Neural Network control of robot manipulators and nonlinear systems*. Taylor & Francis, 1999.

[37] K. Vamvoudakis and F. L. Lewis, "On-line actor-critic algorithm to solve the continuous-time infinite horizon optimal control problem," *Automatica*, vol. 46, pp. 878–888, 2010.

[38] W. Yu and A. Perrusquía, "Simplified stable admittance control using end-effector orientations," *International Journal of Social Robotics*, vol. 12, no. 5, pp. 1061–1073, 2020.

[39] A. Perrusquía, "Solution of the linear quadratic regulator problem of black box linear systems using reinforcement learning," *Information Sciences*, vol. 595, pp. 364–377, 2022.

[40] E. G. Hernandez-Martinez, G. Fernandez-Anaya, E. Ferreira, J. J. Flores-Godoy, and A. Lopez-Gonzalez, "Trajectory tracking of a quadcopter uav with optimal translational control," *IFAC-PapersOnLine*, vol. 48, no. 19, pp. 226–231, 2015.

2023-02-22

Closed-loop output error approaches for þÿdrone s physics informed traje

Perrusquía, Adolfo

IEEE

þÿPerrusquia A, Guo W. (2023) Closed-loop output error approaches for dr
informed trajectory inference. IEEE Transactions on Automatic Control, Volume 68, Issue 12,
December 2023, pp. 7824-7831
https://doi.org/10.1109/TAC.2023.3247461